

# Titanium abundances in late-type stars

## I. 1D non-LTE modelling in benchmark dwarfs and giants

J. W. E. Mallinson<sup>1</sup>, K. Lind<sup>1</sup>, A. M. Amarsi<sup>2</sup>, P. S. Barklem<sup>2</sup>, J. Gruber<sup>2</sup>, A. K. Belyaev<sup>3</sup>, K. Youakim<sup>1</sup>

<sup>1</sup> Department of Astronomy, Stockholm University, AlbaNova University Centre, SE-106 91 Stockholm, Sweden  
e-mail: jack.mallinson@astro.su.se

<sup>2</sup> Theoretical Astrophysics, Department of Physics and Astronomy, Uppsala University, Box 516, SE-751 20 Uppsala, Sweden

<sup>3</sup> Department of Theoretical Physics and Astronomy, Herzen University, St. Petersburg 191186 Russia

### ABSTRACT

**Context.** The titanium abundances of late-type stars are important tracers of Galactic formation history. However, abundances inferred from Ti I and Ti II lines can be in stark disagreement in very metal-poor giants. Departures from local thermodynamic equilibrium (LTE) have a large impact on the minority neutral species and thus influences the ionisation imbalance, but satisfactory non-LTE modelling for both dwarfs and giants has not been achieved in previous literature.

**Aims.** The reliability of titanium abundances is reassessed in benchmark dwarfs and giants using a new non-LTE model and one-dimensional (1D) model atmospheres.

**Methods.** A comprehensive model atom was compiled with a more extended level structure and newly published data for inelastic collisions between Ti I and neutral hydrogen.

**Results.** In 1D LTE, the Ti I and Ti II lines agree to within 0.06 dex for the Sun, Arcturus, and the very metal-poor stars HD84937 and HD140283. For the very metal-poor giant HD122563, the Ti I lines give an abundance that is 0.47 dex lower than that from Ti II. The 1D non-LTE corrections can reach +0.4 dex for individual Ti I lines and +0.1 dex for individual Ti II lines, and reduce the overall ionisation imbalance to −0.17 dex for HD122563. However, it also increases the imbalance for the very metal-poor dwarf and sub-giant to around 0.2 dex.

**Conclusions.** Using 1D non-LTE reduces the ionisation imbalance in very metal-poor giants but breaks the balance of other very metal-poor stars, consistent with the conclusions in earlier literature. To make further progress, consistent 3D non-LTE models are needed.

**Key words.** atomic processes — radiative transfer — line: formation — Stars: abundances — Stars: late-type

## 1. Introduction

In the era of the ESA *Gaia* mission (Gaia Collaboration et al. 2016) and large spectroscopic datasets from current and upcoming million-star surveys like LAMOST (Zhao et al. 2012), APOGEE (Majewski et al. 2017), WEAVE (Dalton et al. 2018), 4MOST (de Jong et al. 2019), and GALAH (Buder et al. 2021), precision spectroscopy is becoming increasingly important to understand the history and evolution of the Milky Way due to the accuracy and detail of the information being received. For example, current and future observations of stars with peculiar chemical abundance patterns, especially in the metal-poor regime, shed light on the assembly of the early Galaxy and its enrichment by supernovae explosions (Nissen & Gustafsson 2018; Helmi 2020).

In this context, titanium is an element of high astrophysical interest. Ti I and Ti II lines are observed throughout a wide range of stars and produce numerous spectral lines. Thus, they are commonly used to calculate titanium abundances and fundamental stellar parameters such as effective temperature ( $T_{\text{eff}}$ ), surface gravity ( $\log(g)$ ), and can also be a proxy for metallicity. Moreover, as an  $\alpha$ -element titanium abundances can trace stars of different ages (Nissen et al. 2020) due to the titanium output difference between Type Ia and core-collapse supernovae. Hence, the Galactic thin and thick discs separate out in the [Ti/Fe] versus [Fe/H] plane (Bensby et al. 2014). As such, accurate titanium

abundance measurements can give insight into the formation and evolution of the Galaxy.

The success of these types of studies critically depends on the accuracy of the inferred titanium abundances. In late-type stars, it is usually possible to infer titanium abundances from both Ti I and Ti II lines. The level of ionisation balance,  $\Delta_{\text{I-II}} \equiv A(\text{Ti})_{\text{Ti I}} - A(\text{Ti})_{\text{Ti II}}$ , can therefore be measured, with non-zero values indicative of some deficiency in the spectral models.

One such deficiency could be the assumption of local thermodynamic equilibrium (LTE), as commonly assumed in classical spectroscopic analyses. In this approximation, the populations of excited and ionised states of titanium follow the Saha-Boltzmann distributions. In reality, similarly to neutral iron, the neutral minority species is prone to departures from LTE: the supra-thermal ultraviolet (UV) radiation field typically leads to overionisation (Bergemann 2011). This effect grows towards lower metallicities where UV photons can travel through the atmosphere with even less impediment, thus both the excess radiation and the LTE error increases.

For example, Scott et al. (2015) find  $\Delta_{\text{I-II}} = -0.15$  dex for the Sun when using a three-dimensional (3D) hydrodynamic model solar atmosphere and 3D LTE radiative transfer. By employing non-LTE corrections computed on a (3D) model atmosphere, Scott et al. (2015) find better agreement between the two species,  $\Delta_{\text{I-II}} = -0.09$  dex. As the authors discuss, consistent 3D non-LTE modelling using improved data for inelastic collisions with

neutral hydrogen may be needed to fully resolve these remaining ionisation imbalances.

For stars other than the Sun, all titanium abundance analyses to date have been based on 1D model atmospheres. In the absence of 3D non-LTE models, 1D non-LTE is expected to be more reliable than 1D LTE and 3D LTE, at least for neutral iron (Amarsi et al. 2016; Nordlander et al. 2017). The most comprehensive 1D non-LTE models to date were recently presented by Sitnova et al. (2020). The authors used the 1D non-LTE code DETAIL (Przybilla et al. 2011) and employed a large model atom utilising, for the first time, *ab initio* inelastic hydrogen collisions. For the Sun, they find  $\Delta_{\text{I-II}} = -0.07$  in 1D LTE, which is in fact similar to the 1D LTE results presented by Scott et al. (2015). Sitnova et al. (2020) find this improves to  $-0.03$  dex in 1D non-LTE.

However, there are larger discrepancies in the metal-poor regime. For the very metal-poor giant HD122563, Sitnova et al. (2020) report  $\Delta_{\text{I-II}} = -0.4$  in 1D LTE. This becomes less severe in 1D non-LTE,  $\Delta_{\text{I-II}} = -0.2$ . Unfortunately, 1D non-LTE instead worsens the ionisation imbalance for the other very metal-poor stars. In 1D LTE, they find  $\Delta_{\text{I-II}} = +0.05$  and  $-0.03$  dex for the benchmark stars HD84937 and HD140283; these change to 0.17 and 0.11 dex, respectively.

It is not clear from where exactly the large ionisation imbalances found by Sitnova et al. (2020) in 1D non-LTE originate. In this context, it is important to note that different groups have reported different 1D non-LTE results for other iron-peak elements. In particular, for copper, Shi et al. (2018) report discrepancies of 0.25 dex, 0.38 dex, and 0.69 dex for HD84937, HD140283, and HD122563 respectively, between their 1D non-LTE results and those of Andrievsky et al. (2018). As such, it is worthwhile to test whether the ionisation imbalances can be due to deficiencies in the non-LTE models, rather than for example failures of the 1D model atmospheres.

This work presents an independent 1D non-LTE study of titanium abundances in late-type benchmark stars. Compared to Sitnova et al. (2020), the results presented here are based on a different non-LTE code, a new model atom with higher uncoupled energy levels, and utilising a more up-to-date prescription for the inelastic collisions with neutral hydrogen. This non-LTE model is used in an attempt to solve the imbalance for the Sun, dwarfs, and giants at once. The rest of this article is structured as follows. The non-LTE model is presented in Sect. 2, and the analysis is described in Sect. 3. The results for the Sun, the giant Arcturus, the very metal-poor stars HD84937 and HD140283, and the very metal-poor giant HD122563 are presented in Sect. 4, before concluding in Sect. 5.

## 2. Method

### 2.1. Overview

The non-LTE calculations and theoretical stellar spectra were performed using Balder (Amarsi et al. 2018b). This code is based on Multi3D (Leenaarts & Carlsson 2009) with updates to the parallelisation scheme and background opacities (Amarsi et al. 2018b) and statistical equilibrium solver (Amarsi et al. 2019).

The following Sects 2.2–2.5 describe the raw data based on which the model atom was constructed. Sect. 2.6 then describes the reduction process of the atom. In summary, the reduced model atom, illustrated in Fig. 1, contains the following:

- 587 energy levels. Of which, 459 are of Ti I, 127 are of Ti II, and the ground state of Ti III is also included.

- 4 784 bound-bound radiative transitions.
- 586 photo-ionisation transitions.

### 2.2. Energy levels

The predicted and observed energy levels of Ti I and Ti II were taken from Kurucz (2016)<sup>1,2</sup> which was also used by Sitnova et al. (2020) and are included in the VALD3 (Ryabchikova et al. 2015) database. Specifically, the files called gf220X.gam and gf220X.lin were used, where X is 0 or 1. The Kurucz (2016) database contains nearly 18 000 bound fine-structure levels for Ti I and Ti II. These level data were combined and reduced as discussed in Sect. 2.6.

### 2.3. Radiative transitions

Data for around six million bound-bound transitions were extracted from Kurucz (2016). This dataset contains more than five million transitions for Ti I alone. These data were reduced as described in Sect. 2.6. For a subset of lines, experimentally measured *f*-values from Wood et al. (2013) and Lawler et al. (2013) were used. These are the same lines that were used for the abundance analysis in Sect. 3.

Photo-ionisation cross-sections for Ti I were adopted from the Nahar (2020) database<sup>3</sup>. Levels from Kurucz (2016) were cross-referenced to match the NORAD database for the initial and target states of photo-ionisation transitions from Nahar (2020) by comparing their electron configurations and terms. Unique matches were found for all but 167 highly excited Ti I levels in the reduced model atom, of which none had an energy below 3.7 eV, and the majority were above 6.2 eV. For these unmatched levels, the hydrogenic approximation was used (Mihalas 1978).

### 2.4. Inelastic hydrogen collisions

Inelastic hydrogen collision data are needed for both bound-bound and charge transfer processes. They are particularly important for metal-poor stellar atmospheres due to the lower electron densities. Therefore, changes in hydrogen collision rate coefficients may have a large impact on the spectra produced. The impact of hydrogen collision processes on the spectra and thus the abundances derived has been shown to be important for other elements (Bergemann & Gehren 2008; Lind et al. 2009; Osorio et al. 2015; Amarsi et al. 2018a; Reggiani et al. 2019; Amarsi et al. 2019; Sitnova et al. 2022).

Initial studies of the non-LTE effects on titanium in stellar atmospheres (Bergemann 2011; Sitnova et al. 2016) were carried out using the Drawin formula (Drawin 1968, 1969; Steenbock & Holweger 1984; Lambert 1993), allowing a scaling factor  $S_{\text{H}}$  to be chosen to minimise the scatter in derived abundances across observed lines in the Sun. These works found that describing the hydrogen collisions in this manner did not work well for metal-poor ( $[\text{Fe}/\text{H}] < -2$ ) stars, giving an ionisation imbalance between Ti I and Ti II, that was larger than found later using quantum mechanical calculations for hydrogen collisions (Sitnova et al. 2020). This is not unexpected, due to the large discrepancy between the Drawin formula results and those from full quantum mechanical calculations (Barklem et al. 2011).

<sup>1</sup> [kurucz.harvard.edu/atoms/2200](http://kurucz.harvard.edu/atoms/2200)

<sup>2</sup> [kurucz.harvard.edu/atoms/2201](http://kurucz.harvard.edu/atoms/2201)

<sup>3</sup> <https://norad.astronomy.osu.edu/>

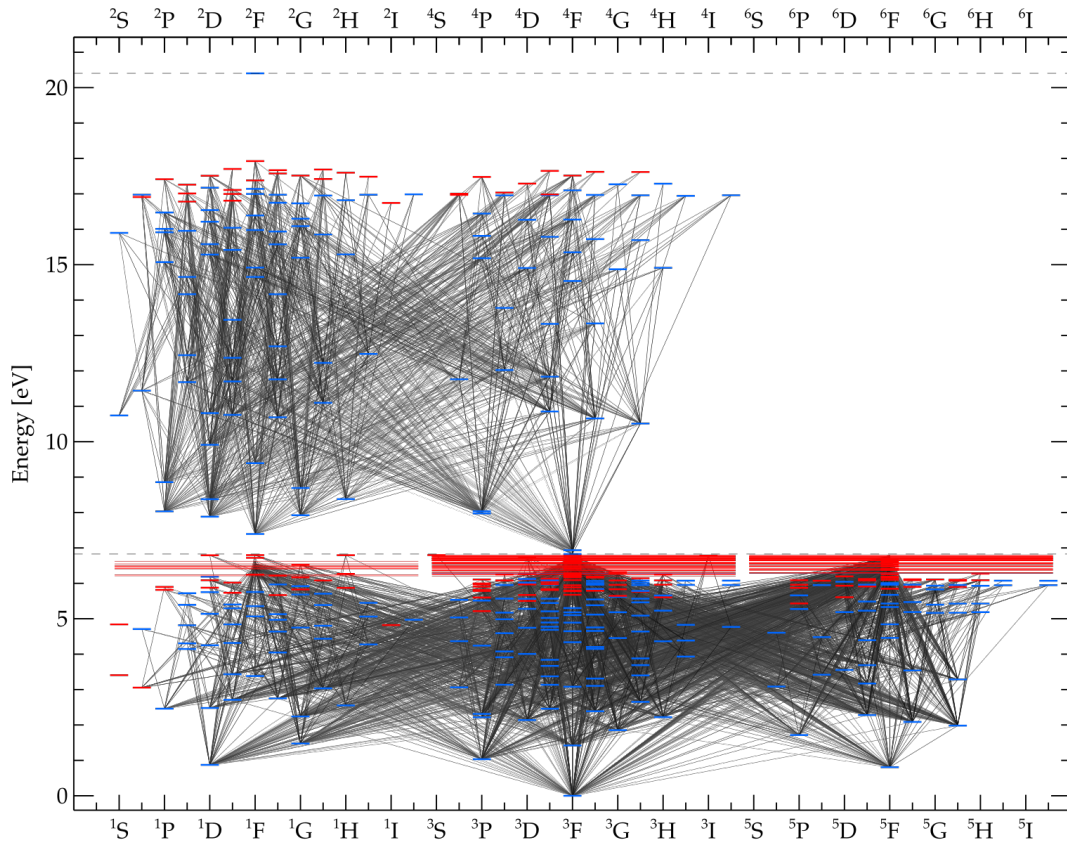


**Fig. 1.** Term diagram of the reduced atom showing the energies for possible bound-bound transitions of Ti I (lower half) and Ti II (upper half). Transitions are shown by black lines, with darker lines representing a higher oscillator strength. Blue marks show the observed energy levels, and red marks show levels that are theoretically predicted.

Unfortunately, full quantum mechanical calculations of such processes are to date only available for neutral lithium (Belyaev & Barklem 2003; Barklem et al. 2003), sodium (Belyaev et al. 1999; Barklem et al. 2010; Belyaev et al. 2010), magnesium (Belyaev et al. 2012; Barklem et al. 2012; Guitou et al. 2015), and calcium (Belyaev et al. 2019). For other species, especially more complex atoms, one must resort to asymptotic model calculations based on simplified electronic structure and collision dynamics. Such approaches include the asymptotic model of Belyaev (2013), the asymptotic model of Barklem (2016), the simplified method of Belyaev et al. (2017) and also of Belyaev & Voronov (2018). The asymptotic model of Barklem (2016) is based on linear combinations of atomic orbitals (LCAO) for the ionic-covalent interactions at avoided ionic crossings, expected to be the dominant mechanism where applicable. The others are based on a fit to calculations where the ionic-covalent interactions are taken from a semi-empirical formula (Olson et al. 1971).

Asymptotic model calculations based on LCAO were carried out for processes on neutral titanium by Grumer & Barklem (2020), while the simplified method was applied in Sitnova et al. (2020) to both neutral and singly ionised titanium. The bound-bound excitation rates for neutral titanium are compared in Fig. 2, and the charge transfer (ion-pair production) rates involving neutral titanium in Fig. 3. In Fig. 3 good agreement can be seen for the most important charge transfer transitions, i.e. those with large rate coefficients. However, the two data sets dif-

fer for processes with low rates, a behaviour also seen for bound-bound processes in Fig. 2. The larger scatter seen in the data from Grumer & Barklem (2020) is due to the explicit consideration of angular momentum coupling in the LCAO approach (i.e. the  $L$  and  $S$  quantum numbers in  $LS$  coupling), which is not treated in the simplified approach.

In this work, the collision rate coefficients for bound-bound transitions in Ti I and its charge transfer rates to Ti II were taken from Grumer & Barklem (2020)<sup>4</sup>, and Ti II bound-bound rates were taken from Sitnova et al. (2020)<sup>5</sup>. This resulted in data for the most important, but not all, transitions. For bound-bound transitions in Ti I involving states above the ionic limit, i.e. where the energy is within 0.754 eV (the electron affinity of hydrogen) of the ionised ground state, the ionic crossing mechanism does not apply, and an alternate mechanism must be at work. In these cases, the Kaulakys (1991) free electron model can be used to estimate the cross-sections and rate coefficients, via a momentum transfer mechanism. It has been argued in earlier work (Amarsi et al. 2018a) that the contribution from this mechanism should be added to the ionic crossing contribution, though the validity of the free electron model for low-lying states is questionable. The results of the free electron model calculations for all bound-bound transition are shown in Fig. 4, and compared to Grumer & Barklem (2020). Following Amarsi et al. (2018a) the two con-

<sup>4</sup> <https://github.com/barklem/public-data>

<sup>5</sup> [http://www.non-lte.com/ti\\_h.html](http://www.non-lte.com/ti_h.html)



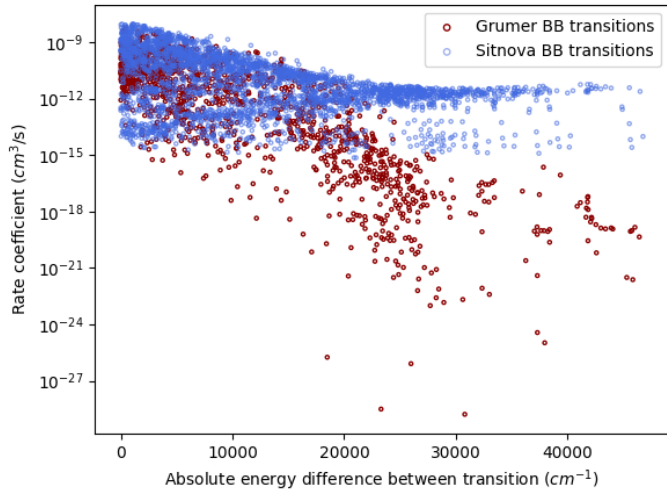


**Fig. 2.** Ti I bound-bound de-excitation rate coefficients as a function of the energy difference between transitions. Red points are from Grumer & Barklem (2020), and blue points are from Sitnova et al. (2020).

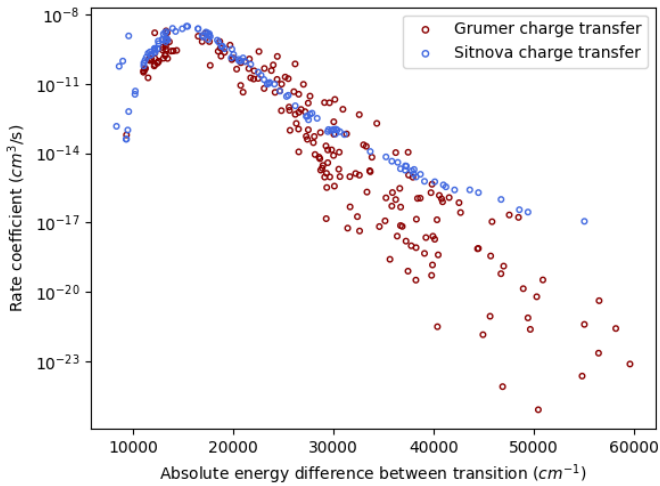


**Fig. 3.** Comparison of charge transfer rates for the reaction  $\text{Ti I} + \text{H} \rightarrow \text{Ti II} + \text{H}^-$ . Red points show data from Grumer & Barklem (2020) and blue points are from Sitnova et al. (2020), as in Fig. 2.

tributions are added together and their impact on abundance was found to be below 0.1 dex in all stars.

## 2.5. Electron collisions

Titanium has no advanced quantum mechanical data for electron collisions for a majority of states, and so all transitions were calculated using the semi-empirical recipes from van Regemorter (1962) for excitation and Cox (2000) for ionisation. Due to the dominance of hydrogen collisions, especially in metal-poor stars, the approximations made for electrons are found to have a small impact on the resulting abundances.

## 2.6. Atom reduction

The complete model atom contains thousands of levels and millions of radiative transitions, and required reduction in order to make the non-LTE calculations feasible, even in 1D. To begin with, all fine structure was removed. Moreover, Ti I levels above 6.2 eV with identical parity, electron configuration, and multiplicity were merged to form super-levels, and affected lines

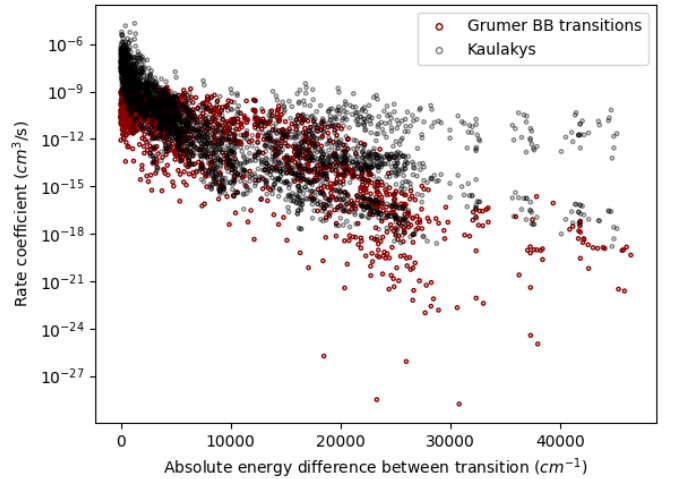


**Fig. 4.** Comparison between de-excitation rate coefficients from Grumer & Barklem (2020) (red points) and the rates calculated using the Kaulakys code for the same transitions (black points). The same relationship is found here as in Amarsi et al. (2018a).

merged to form super-lines, following Lind et al. (2017). This created a smaller atom of 587 total energy levels and 50 000 transitions, that was still too large to be practical. Ti II levels within 2.7 eV to the ionisation limit were cut, due to their low population in late-type stellar atmospheres.

Further reductions were made by considering the radiative brackets  $|n_i R_{ij} - n_j R_{ji}|$  for different bound-bound radiative transitions. This quantity gives an estimate of the relative importance of a radiative transition to the statistical equilibrium: the lower the value, the less important it is and the safer it is to remove it. While this requires an individual depth point to be chosen, the choice does not exert much influence on the overall transition hierarchy (Lind et al. 2017). By comparing the radiative bracket of the Sun and HD84937, 4 784 of the most important bound-bound radiative transitions were selected, and the rest were discarded, resulting in the final reduced atom.

To reduce the computational cost further, the photo-ionisation cross-sections were interpolated onto a common wavelength grid with fixed logarithmic steps, reducing the number of unique wavelength values from over 3 million to just over 38 000. This reduced computation time and memory requirements as, although the total number of wavelengths did not vary dramatically, it allowed Balder to treat each set of identical wavelength values as a single one during the run. While unlikely to cause a significant change, the accuracy of the interpolation was checked in two ways: First, by removing 10% of Nahar (2015) data before interpolation, re-calculating their values, and comparing these to the original cross-sections of the removed data; secondly, by manual inspection when interpolating all wavelengths to ensure all resonances and features were still retained in the interpolated model.

The final reduced atom is illustrated in Fig. 1, which demonstrates the complexity of the atom, even after collapsing levels. It contains 459 Ti I levels under its ionisation potential of 6.828 eV, 127 Ti II levels that reach up to 2.5 eV below the ionisation limit, and the Ti III ground state. This atom was run in non-LTE to produce the departure coefficients,  $n_{\text{NLTE}}/n_{\text{LTE}}$ , shown in Fig. 5. When generating synthetic spectra for diagnostic spectral lines, the departure coefficients were redistributed onto the complete model atom that contains fine structure, but with the theoretical levels removed.

**Table 1.** Stellar parameters of the studied benchmark stars.

Star	$T_{\text{eff}}$ K	$\log(g)$ $\text{cm s}^{-2}$	[Fe/H]	$\xi$ $\text{km s}^{-1}$	Ref.
Sun	5772	4.44	0.00	0.9	a, d
Arcturus	4286	1.64	−0.53	1.3	b, d
HD84937	6356	4.06	−2.06	1.2	b, d
HD140283	5792	3.65	−2.36	1.3	c, d
HD122563	4636	1.40	−2.50	1.8	c, d

**Notes.** <sup>(a)</sup> Solar  $T_{\text{eff}}$  and  $\log(g)$  from Prša et al. (2016). <sup>(b)</sup>  $T_{\text{eff}}$  and  $\log(g)$  from Heiter et al. (2015). <sup>(c)</sup>  $T_{\text{eff}}$  and  $\log(g)$  from Karovicova et al. (2020). <sup>(d)</sup> [Fe/H] and  $\xi$  from Lind et al. (2022).

### 2.7. Atom comparison

This atom contains more unmerged levels than used previously in Sitnova et al. (2020), to examine the influence these high energy levels have on titanium abundance predictions. More levels are also coupled with hydrogen collisions via the use of the Kaulakys principle for the higher energy levels above the ionic limit of Ti I. The average  $f$ -values are calculated in this paper using the experimental data of Wood et al. (2013) and Lawler et al. (2013) where possible, whereas Sitnova et al. (2020) used the database of R. Kurucz, although it was stated that the comparison was made, and the shift found to be minor, at an average of  $\log(gf_{\text{lab}}) - \log(gf_{\text{Kurucz}}) = -0.05 \pm 0.28$  dex.

## 3. Analysis of Benchmark stars

Five well-known benchmark stars were analysed using high-resolution optical spectra for the Sun, Arcturus, HD84937, HD140283, and HD122563. The same observational data used in Scott et al. (2015) was used for the Sun, and the observational data from Lind et al. (2022) was used for all other stars. The same stellar parameters were adopted as in that work, shown in Table 1. In summary, Lind et al. (2022) used interferometric  $T_{\text{eff}}$  for Arcturus, HD122563, and HD140283, while  $T_{\text{eff}}$  for HD84937 was calculated from its surface-brightness relationship (Heiter et al. 2015). Except for the Sun,  $\log(g)$  was computed from mass to radius relations for all stars. [Fe/H] and microturbulence parameters were adopted from Lind et al. (2022), who determined them simultaneously by enforcing a flat trend in LTE abundance and equivalent width of Fe II lines. The atmospheres were tailored for each star by interpolating (Masseron 2006) a grid standard of MARCS models (Gustafsson et al. 2008) onto these stellar parameters.

The line selection of titanium can play a large role in some abundance calculations due to uncertain oscillator strengths, blends, as well as difficulties associated with core saturation. Measures were taken to reduce the impact of these on the overall estimates of titanium abundances, and the final choices shown in Table A.1. The impact of uncertain oscillator strengths was mitigated by using a large selection of lines, assuming the uncertainties to be normally distributed. Spectral lines were fit with one or several Gaussian profile following Lind et al. (2022), from which their equivalent widths were determined, with blended lines removed essentially via sigma-clipping. Saturated lines were removed by imposing a limit on the reduced equivalent width of  $W_{\lambda, \text{red}} = \log_{10}(W_{\lambda}/\lambda) = -4.9$ . The final line selection closely resembles that of Scott et al. (2015) for the Sun, Heiter et al.

(2015) for Arcturus, and Wood et al. (2013) and Lawler et al. (2013) for the very metal-poor stars. 13–37 Ti I lines and 3–92 Ti II lines were used, depending on the star.

## 4. Results

### 4.1. Overview

As anticipated, non-LTE is found to, in general, reduce the strengths of Ti I lines, consistent with overionisation. The departure coefficients for the levels lie below 0 (Fig. 5). This translates to positive non-LTE abundance corrections for this species, increasing the titanium abundances inferred from these lines. Compared to Sitnova et al. (2020), Fig. 5 misses several Ti II lines that extend to large departure coefficients. Indeed, this work finds smaller non-LTE effects for Ti II as this would indicate, as it shows a closer coupling to the LTE value of  $\log_{10}(\beta) = 0$ .

The non-LTE corrections are found to be largest for the very metal-poor giant HD122563, where they can reach over +0.4 dex for certain Ti I lines. For the very metal-poor dwarf and sub-giant, the non-LTE corrections are of the order +0.2 dex. For the Sun, the corrections are more muted, only of the order +0.05 dex. Nevertheless, they make an impact on the ionisation balance Sect. 4.2.1. For Arcturus, the abundance corrections are typically of the order +0.01 dex.

For Ti II, the non-LTE corrections are smaller. They can be positive or negative, depending on the transition and on the star. The departure coefficients demonstrate that, given the deeper line creation point, they exist closer to LTE in almost all cases. The most severe case is HD122563, where certain lines are affected to the +0.2 dex level, and much smaller in all other stars.

In many stars, but most particularly Arcturus, over saturation was found when analysing the reduced equivalent widths of the lines and their abundance predictions. To counter the inaccurate abundance estimations due to the modified relationship with abundance the saturated lines have, those with a reduced equivalent width of  $\log_{10}(W_{\lambda}/\lambda) > -4.9$  were removed, improving the imbalance in all stars but the Sun in LTE. In Arcturus, this left few Ti II lines, but achieved a better ionisation imbalance nonetheless.

### 4.2. Abundances and ionisation balance

The mean abundances and ionisation imbalances,  $\Delta_{\text{I-II}}$ , are presented in Table 2 and Fig. 6. The different stars are discussed individually below.

The differences from Sitnova et al. (2020) are small in LTE, but significant enough to be noted. This could be attributed in part to the difference in the microturbulence parameters in these stars. In this work, they are found to be 0.5 km/s smaller for HD84937, the same for HD140283, and 0.2 km/s larger for HD122563. Indeed, it is found that the discrepancy in LTE abundances with respect to Sitnova et al. (2020) is largest for HD84937 and HD122563. (Table 2).

#### 4.2.1. The Sun

In the Sun, the 1D LTE abundances are found to be  $4.87 \pm 0.01$  for Ti I and  $4.92 \pm 0.01$  for Ti II, where the uncertainties reflect the standard error in the mean of the set of diagnostic lines. They are in excellent agreement with the results from Scott et al. (2015), who obtained 4.85 and 4.91 respectively in LTE using 1D MARCS models. They are also consistent within errors with the 1D LTE results from Sitnova et al. (2020), 4.88 and 4.95 respectively.

**Table 2.** Titanium abundances,  $A(\text{Ti})$ , and ionisation imbalances,  $\Delta_{\text{I-II}}$ , found in this work as well as the unweighted values in [Ramírez & Allende Prieto \(2011\)](#) for Arcturus, and in [Sitnova et al. \(2020\)](#) for the other stars.

Star	Species	LTE			Non-LTE		
		Here	Lit.	Diff.	Here	Lit.	Diff.
Sun	Ti I	4.87	4.88	-0.01	4.90	4.91	-0.01
	Ti II	4.92	4.95	-0.03	4.92	4.94	-0.02
	$\Delta_{\text{I-II}}$	-0.06	-0.07	0.02	-0.02	-0.03	0.02
Arcturus	Ti I	4.85	4.66	0.19	4.86	—	—
	Ti II	4.93	4.66	0.27	4.91	—	—
	$\Delta_{\text{I-II}}$	-0.08	0.00	-0.08	-0.05	—	—
HD84937	Ti I	3.20	3.19	0.01	3.40	3.35	0.05
	Ti II	3.20	3.14	0.06	3.21	3.18	0.03
	$\Delta_{\text{I-II}}$	0.00	0.05	-0.05	0.18	0.17	-0.01
HD140283	Ti I	2.69	2.66	0.03	2.91	2.84	0.07
	Ti II	2.69	2.69	0.00	2.71	2.73	-0.02
	$\Delta_{\text{I-II}}$	0.00	-0.03	-0.03	0.20	0.11	0.09
HD122563	Ti I	2.09	2.19	-0.10	2.41	2.40	0.01
	Ti II	2.54	2.58	-0.04	2.57	2.60	-0.03
	$\Delta_{\text{I-II}}$	-0.45	-0.40	-0.05	-0.16	-0.20	0.04

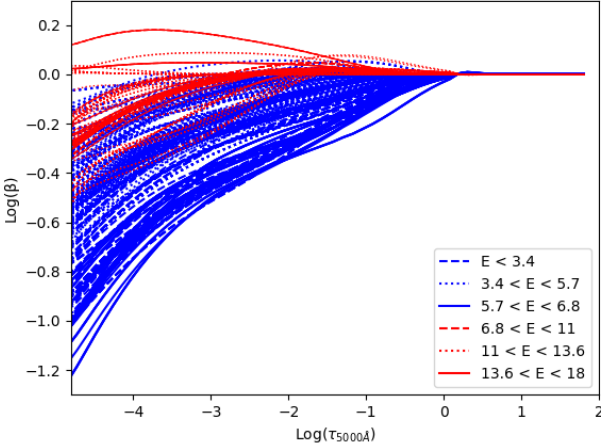


**Fig. 5.** Departure coefficients of titanium in HD84937 as a function of optical depth. Dotted lines represent Ti II and solid lines represent Ti I. It reaches rough agreement with LTE deeper in the star as collisions dominate. Ti II can be seen to be in closer agreement with LTE than Ti I over all energy levels.

With the inclusion of 1D non-LTE effects, the abundances are found to be  $4.90 \pm 0.01$  and  $4.92 \pm 0.01$  for Ti I and Ti II respectively. This is again consistent close to the corresponding abundances in [Sitnova et al. \(2020\)](#), 4.91 and 4.94 respectively.

The 1D LTE abundances correspond to an imbalance of  $\Delta_{\text{I-II}} = -0.06 \pm 0.05$  dex. This is small, but significant, especially given that the solar parameters are known precisely. The 1D non-LTE abundances correspond to a much smaller ionisation imbalance,  $\Delta_{\text{I-II}} = -0.02 \pm 0.05$  dex. These imbalances are slightly smaller in both magnitude and error than [Sitnova et al. \(2020\)](#).

#### 4.2.2. Arcturus

For Arcturus, the 1D LTE titanium abundance is found to be  $4.82 \pm 0.02$  from Ti I lines, and  $4.93 \pm 0.01$  from Ti II lines. In non-LTE, these change to  $4.83 \pm 0.03$  for Ti I and  $4.90 \pm 0.00$  for Ti II. The non-LTE effects for this mildly metal-poor star are small, as was also found for the Sun (Sect. 4.2.1).

In 1D LTE Arcturus has a marginally significant titanium ionisation imbalance of  $\Delta_{\text{I-II}} = -0.08 \pm 0.08$  dex. In non-LTE the results:  $\Delta_{\text{I-II}} = -0.05 \pm 0.08$  dex. The abundances remain slightly higher than literature values of 4.66 dex ([Ramírez & Allende Prieto 2011](#)), which can in part be explained by the higher microturbulence adopted in that work, and their line selection.

#### 4.2.3. Very metal-poor giant: HD122563

For HD122563, the 1D LTE titanium abundances are  $2.09 \pm 0.03$  when inferred from Ti I lines, and  $2.54 \pm 0.02$  from Ti II lines. These values are somewhat lower than the 1D LTE values of [Sitnova et al. \(2020\)](#), who found 2.19 for Ti I and 2.58 for Ti II.

The red giant suffers from the largest non-LTE effects: For Ti I they amount to a correction of +0.32 dex, such that the titanium abundance increases to  $2.41 \pm 0.02$ . For Ti II the overall correction is just +0.03 dex, giving  $2.57 \pm 0.02$  for Ti II. The effects are much larger than those in Arcturus (Sect. 4.2.2) due to the much lower metallicity of HD122563 that leads to greater overionisation.

Although the non-LTE correction on Ti I found here is larger than that found by [Sitnova et al. \(2020\)](#) (+0.21 dex), it turns out that the 1D non-LTE abundances of that work and this are in good agreement, as [Sitnova et al. \(2020\)](#) found 2.40 for Ti I and 2.60 for Ti II.

The 1D LTE ionisation imbalance  $\Delta_{\text{I-II}}$  is found to also be the most severe of all the stars in this sample:  $\Delta_{\text{I-II}} = -0.45 \pm 0.08$  dex. The large non-LTE correction for Ti I, and the correspondingly small correction for Ti II, thus greatly improves this:  $\Delta_{\text{I-II}} = -0.16 \pm 0.08$  dex. Hence, it is found that, although 1D non-LTE improves the ionisation imbalance, it does not completely re-

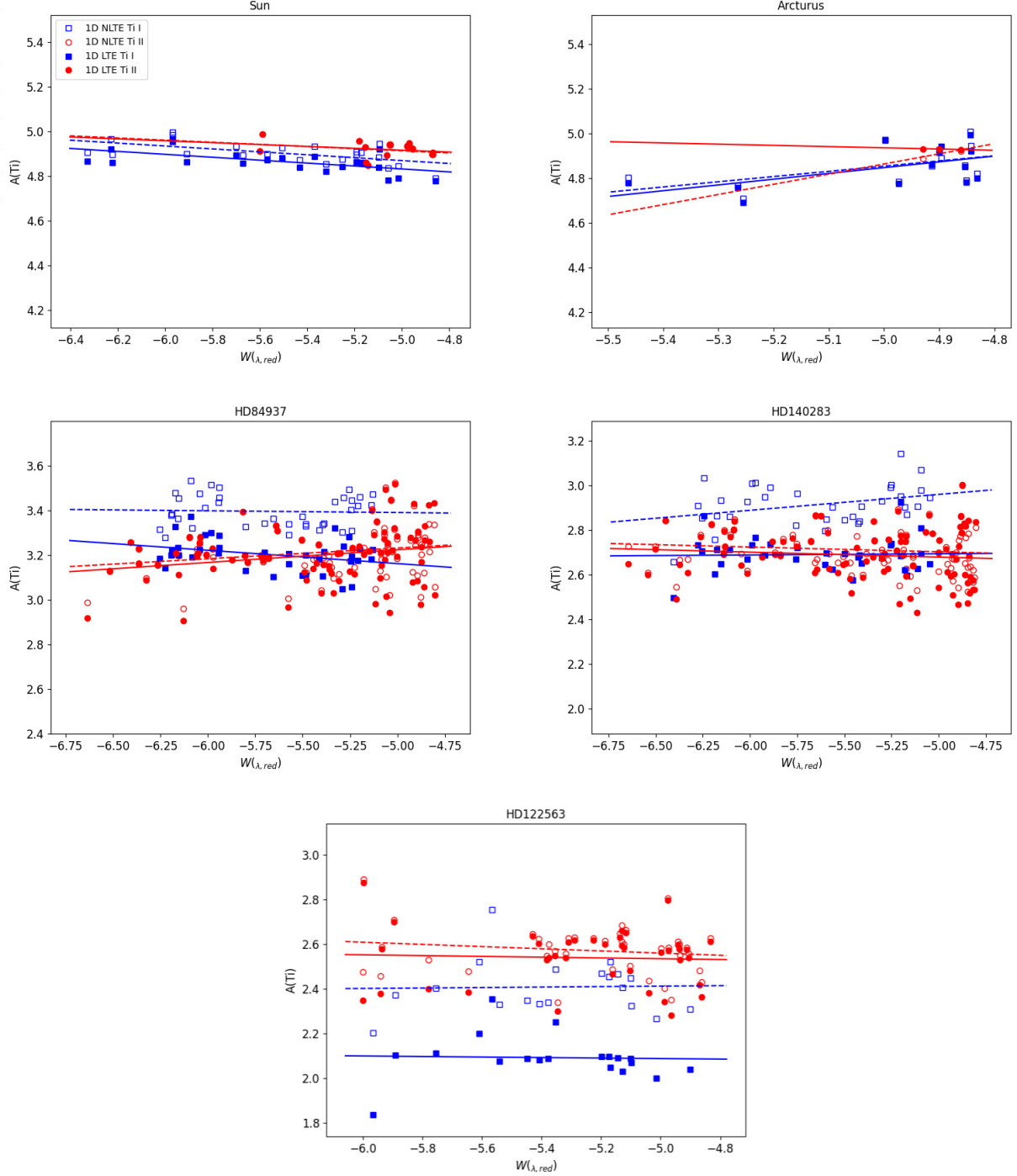


**Fig. 6.** The difference between the mean abundance of Ti I and Ti II in LTE and non-LTE for all stars, representing the ionisation imbalance. Filled symbols represent LTE and empty symbols non-LTE. Red circles and lines show Ti II, and blue squares Ti I. Lines represent the abundance trend, dashed for non-LTE and solid for LTE. The x-axis is reduced equivalent width:  $\log_{10}(W_{\lambda}/\lambda)$ .

move it. This motivates further study beyond 1D non-LTE for red giants. In other words, 3D non-LTE calculations.

#### 4.2.4. Very metal-poor dwarf and subgiant: HD84937 and HD140283

In 1D LTE, the titanium abundance of HD84937 is measured to be  $3.20 \pm 0.01$  from Ti I lines and  $3.20 \pm 0.01$  from Ti II lines. In 1D non-LTE, the Ti I result increases by  $+0.20$  dex to  $3.40 \pm 0.01$ ,

while the Ti II result is almost unchanged at  $3.21 \pm 0.01$ . The correction for Ti I is larger than the  $+0.12$  dex found in [Sitnova et al. \(2020\)](#). Nevertheless, the 1D non-LTE abundances found here are consistent with those in that work, at 3.35 and 3.18 from Ti I and Ti II lines respectively.

The findings for the sub-giant HD140283 are qualitatively similar, with a large 1D non-LTE correction of 0.22 dex for Ti I lines and a smaller one of 0.02 dex for Ti II lines. The 1D non-LTE abundances found here,  $2.91 \pm 0.01$  and  $2.71 \pm 0.01$  respec-



tively, are roughly consistent with those derived by [Sitnova et al. \(2020\)](#), 2.84 and 2.73 respectively.

Titanium ionisation balance is perfectly achieved in 1D LTE for both HD84937 and HD140283:  $\Delta_{\text{I-II}} = 0.00 \pm 0.05$  dex. Since the Ti I lines suffer a considerable non-LTE effect while the Ti II lines are largely unaffected, this means that a significant ionisation imbalance develops in 1D non-LTE:  $\Delta_{\text{I-II}} = 0.18 \pm 0.05$  and  $0.20 \pm 0.05$  dex for the two stars respectively. This was also found in the independent study of [Sitnova et al. \(2020\)](#): 1D non-LTE ionisation imbalances of  $\Delta_{\text{I-II}} = 0.17$  and  $0.11$  dex were found for these two stars respectively, whereas in 1D LTE ionisation balance was achieved to 0.05 dex or better.

## 5. Conclusion

Titanium abundances in late-type stars have been investigated using 1D model atmospheres and LTE and non-LTE radiative transfer. The present work makes use of an extended model atom that includes new quantum data for inelastic collisions with neutral hydrogen. Promisingly, it was found that 1D non-LTE models significantly reduce the ionisation imbalance,  $\Delta_{\text{I-II}}$ , for the Sun (from  $-0.06 \pm 0.05$  to  $-0.02 \pm 0.05$  dex) and the very metal-poor giant HD122563 (from  $-0.47 \pm 0.08$  to  $-0.17 \pm 0.08$  dex), relative to 1D LTE. At the same time, however, 1D non-LTE models worsen the ionisation imbalance for the very metal-poor stars HD84937 and HD140283 respectively (by around 0.2 dex). Titanium lines in the mildly metal-poor giant Arcturus were found to form very close to LTE, for which there remains a small ionisation imbalance ( $-0.08 \pm 0.08$  dex).

These overall conclusions are broadly consistent with what was found previously by [Sitnova et al. \(2020\)](#), although the non-LTE effects are slightly larger for Ti I and smaller for Ti II. This is reassuring, given that the current work uses a different radiative transfer code Balder and a more extended model atom that employs newer data for inelastic Ti I collisions with neutral hydrogen.

It is quite possible that the residual ionisation imbalances for titanium are in part driven by 3D effects, which are significant for the Sun ([Scott et al. 2015](#)). The effect may be expected to be even larger for metal-poor stars, for which the steep temperature gradients should enhance the non-LTE overionisation effects ([Amarsi et al. 2016](#); [Nordlander et al. 2017](#)).

Further insight may be gained by comparison to Fe, for which 1D and 3D non-LTE calculations have been performed. Several studies have found reasonable ionisation balances for HD84937 and HD140283 in 1D non-LTE using either the Drawin formula ([Zhao et al. 2016](#)) or asymptotic models like those employed in this work ([Amarsi et al. 2016](#)). However, for HD122563, [Amarsi et al. \(2016\)](#) report an ionisation imbalance of around  $\Delta_{\text{Fe I-Fe II}} = 0.3$  dex in both 1D and 3D non-LTE, similar to the imbalance found in this work for titanium. This may point to yet unidentified shortcomings for metal-poor giants, but a larger sample of stars should be analysed before firm conclusions can be drawn. In any case, 3D non-LTE calculations for titanium will aid in the understanding of these problems.

**Acknowledgements.** JM and KL acknowledge funds from the European Research Council (ERC) under the European Union's Horizon 2020 research and innovation programme (Grant agreement No. 852977). AMA, JG and PSB acknowledge support from the Swedish Research Council through individual project grants with contract Nos. 2020-03940, 2020-05467 and 2020-03404. This work has made use of the VALD database, operated at Uppsala University, the Institute of Astronomy RAS in Moscow, and the University of Vienna. AKB gratefully acknowledges support from the Russian Science Foundation (the Russian Federation), Project No 22-23-01181.

## References

- Amarsi, A. M., Barklem, P. S., Asplund, M., Collet, R., & Zatsarinny, O. 2018a, *A&A*, 616, A89
- Amarsi, A. M., Barklem, P. S., Collet, R., Grevesse, N., & Asplund, M. 2019, *A&A*, 624, A111
- Amarsi, A. M., Lind, K., Asplund, M., Barklem, P. S., & Collet, R. 2016, *MNRAS*, 463, 1518
- Amarsi, A. M., Nordlander, T., Barklem, P. S., et al. 2018b, *A&A*, 615, A139
- Andrievsky, S., Bonifacio, P., Caffau, E., et al. 2018, *MNRAS*, 473, 3377
- Barklem, P., Belyaev, A., Guitou, M., et al. 2011, *Astronomy & Astrophysics - ASTRON ASTROPHYS*, 530
- Barklem, P. S. 2016, *Phys. Rev. A*, 93, 042705
- Barklem, P. S., Belyaev, A. K., & Asplund, M. 2003, *Astronomy and Astrophysics*, 409
- Barklem, P. S., Belyaev, A. K., Dickinson, A. S., & Gad  a, F. X. 2010, *A&A*, 519, A20
- Barklem, P. S., Belyaev, A. K., Spielfiedel, A., Guitou, M., & Feautrier, N. 2012, *A&A*, 541, A80
- Belyaev, A., Vlasov, D., Mitrushchenkov, A., & Feautrier, N. 2019, *Monthly Notices of the Royal Astronomical Society*, 490, 3384
- Belyaev, A. K. 2013, *Phys. Rev. A*, 88, 052704
- Belyaev, A. K. & Barklem, P. S. 2003, *Phys. Rev. A*, 68, 062703
- Belyaev, A. K., Barklem, P. S., Dickinson, A. S., & Gad  a, F. X. 2010, *Phys. Rev. A*, 81, 032706
- Belyaev, A. K., Barklem, P. S., Spielfiedel, A., et al. 2012, *Phys. Rev. A*, 85, 032704
- Belyaev, A. K., Grosser, J., Hahne, J., & Menzel, T. 1999, *Phys. Rev. A*, 60, 2151
- Belyaev, A. K. & Voronov, Y. V. 2018, *ApJ*, 868, 86
- Belyaev, A. K., Yakovleva, S. A., & Kraemer, W. P. 2017, *European Physical Journal D*, 71, 276
- Bensby, T., Feltzing, S., & Oey, M. S. 2014, *A&A*, 562, A71
- Bergemann, M. 2011, *Monthly Notices of The Royal Astronomical Society - MON NOTIC ROY ASTRON SOC*, 413
- Bergemann, M. & Gehren, T. 2008, *Astronomy & Astrophysics*, 492, 823
- Buder, S., Sharma, S., Kos, J., et al. 2021, *MNRAS*, 506, 150
- Cox, A. N. 2000, *Allen's astrophysical quantities* (New York : AIP Press : Springer)
- Dalton, G., Trager, S., Abrams, D. C., et al. 2018, in *Society of Photo-Optical Instrumentation Engineers (SPIE) Conference Series*, Vol. 10702, 107021B
- de Jong, R. S., Agertz, O., Berbel, A. A., et al. 2019, *The Messenger*, 175, 3
- Drawin, H.-W. 1968, *Zeitschrift f  r Physik A Hadrons and nuclei*, 211, 404
- Drawin, H. W. 1969, *Z. Phys.*, 225: 483-93(1969).
- Gaia Collaboration, Prusti, T., de Bruijne, J. H. J., et al. 2016, *A&A*, 595, A1
- Grumer, J. & Barklem, P. S. 2020, *Astronomy & Astrophysics*, 637, A28
- Guitou, M., Spielfiedel, A., Rodionov, D., et al. 2015, *Chemical Physics*, 462, 94
- Gustafsson, B., Edvardsson, B., Eriksson, K., et al. 2008, *A&A*, 486, 951
- Heiter, U., Jofr  , P., Gustafsson, B., et al. 2015, *A&A*, 582, A49
- Helmi, A. 2020, *ARA&A*, 58, 205
- Karovicova, I., White, T. R., Nordlander, T., et al. 2020, *A&A*, 640, A25
- Kaulakys, B. 1991, 24, L127
- Kurucz, R. L. 2016, Robert L. Kurucz on-line database of observed and predicted atomic transitions
- Lambert, D. L. 1993, *Physica Scripta Volume T*, 47, 186
- Lawler, J. E., Guzman, A., Wood, M. P., Sneden, C., & Cowan, J. J. 2013, *ApJS*, 205, 11
- Leenaarts, J. & Carlsson, M. 2009, in *Astronomical Society of the Pacific Conference Series*, Vol. 415, *The Second Hinode Science Meeting: Beyond Discovery-Toward Understanding*, ed. B. Lites, M. Cheung, T. Magara, J. Mariska, & K. Reeves, 87
- Lind, K., Amarsi, A. M., Asplund, M., et al. 2017, *MNRAS*, 468, 4311
- Lind, K., Asplund, M., & Barklem, P. S. 2009, *A&A*, 503, 541
- Lind, K., Nordlander, T., Wehrhahn, A., et al. 2022, *Non-LTE abundance corrections for late-type stars from 2000   to 3  m: I. Na, Mg, and Al*
- Majewski, S. R., Schiavon, R. P., Frinchaboy, P. M., et al. 2017, *AJ*, 154, 94
- Masseron, T. 2006, PhD thesis, Obs. de Paris
- Mihalas, D. 1978, *Stellar atmospheres*
- Nahar, S. 2015, *New Astronomy*, 38
- Nahar, S. 2020, *Atoms*, 8, 68
- Nissen, P. E., Christensen-Dalsgaard, J., Mosumgaard, J. R., et al. 2020, *A&A*, 640, A81
- Nissen, P. E. & Gustafsson, B. 2018, *A&A Rev.*, 26, 6
- Nordlander, T., Amarsi, A. M., Lind, K., et al. 2017, *A&A*, 597, A6
- Olson, R., Smith, F., & Bauer, E. 1971, *Applied Optics*, 10, 1848
- Osorio, Y., Barklem, P. S., Lind, K., et al. 2015, *A&A*, 579, A53
- Przybilla, N., Nieva, M.-F., & Butler, K. 2011, in *Journal of Physics Conference Series*, Vol. 328, *Journal of Physics Conference Series*, 012015
- Pr  a, A., Harmanec, P., Torres, G., et al. 2016, *The Astronomical Journal*, 152, 41
- Ram  rez, I. & Allende Prieto, C. 2011, *The Astrophysical Journal*, 743, 135



- Reggiani, H., Amarsi, Anish M., Lind, Karin, et al. 2019, *A&A*, 627, A177
- Ryabchikova, T., Piskunov, N., Kurucz, R. L., et al. 2015, *Phys. Scr*, 90, 054005
- Scott, P., Asplund, Martin, Grevesse, Nicolas, Bergemann, Maria, & Jacques Sauval, A. 2015, *A&A*, 573, A26
- Shi, J. R., Yan, H. L., Zhou, Z. M., & Zhao, G. 2018, *ApJ*, 862, 71
- Sitnova, T. M., Mashonkina, L. I., & Ryabchikova, T. A. 2016, *Monthly Notices of the Royal Astronomical Society*, 461, 1000
- Sitnova, T. M., Yakovleva, S. A., Belyaev, A. K., & Mashonkina, L. I. 2020, *Astronomy Letters*, 46, 120
- Sitnova, T. M., Yakovleva, S. A., Belyaev, A. K., & Mashonkina, L. I. 2022, *Monthly Notices of the Royal Astronomical Society*, 515, 1510
- Steenbock, W. & Holweger, H. 1984, *Astronomy and Astrophysics*, 130, 319
- van Regemorter, H. 1962, *ApJ*, 136, 906
- Wood, M. P., Lawler, J. E., Sneden, C., & Cowan, J. J. 2013, *The Astrophysical Journal Supplement Series*, 208, 27
- Zhao, G., Mashonkina, L., Yan, H. L., et al. 2016, *ApJ*, 833, 225
- Zhao, G., Zhao, Y.-H., Chu, Y.-Q., Jing, Y.-P., & Deng, L.-C. 2012, *Research in Astronomy and Astrophysics*, 12, 723

## Appendix A: Additional Table

This section contains the linelists used for both Ti I and Ti II in each star individually, and the necessary information on each transition in the model atom.

**Table A.1.** Lines considered in the analysis, including saturated lines that were removed during final abundance calculation. Error for equivalent widths was not available for the lines of the Sun from [Scott et al. \(2015\)](#).

Wavelength Å	$E_{exc}$ eV	$\log(gf)$	$W_\lambda$ mÅ	Error	Abundances	
					LTE	NLTE
Sun						
Ti I						
4281.367	0.818	-1.038	24.000	—	4.84	4.87
4465.805	1.749	0.016	35.600	—	4.84	4.88
4758.118	2.250	0.168	41.800	—	4.78	4.83
4759.270	2.267	0.430	46.000	—	4.79	4.84
5022.868	0.836	-0.221	69.900	—	4.78	4.78
5113.440	1.460	-0.591	24.500	—	4.82	4.85
5145.460	1.502	-0.540	33.100	—	4.86	4.89
5147.478	0.021	-1.794	34.600	—	4.86	4.90
5152.184	0.048	-1.841	33.200	—	4.86	4.90
5219.702	0.048	-2.111	22.400	—	4.89	4.93
5252.100	0.813	-2.837	16.400	—	4.88	4.92
5295.776	1.430	-1.590	10.600	—	4.89	4.93
5490.148	1.502	-0.840	20.300	—	4.84	4.87
6092.792	1.968	-1.722	3.600	—	4.92	4.96
6258.102	1.460	-0.281	50.500	—	4.92	4.94
6303.757	1.460	-1.471	6.800	—	4.97	5.00
6312.236	1.502	-1.550	6.800	—	4.95	4.98
7357.727	1.460	-0.911	19.900	—	4.87	4.89
8675.372	1.430	-1.500	18.500	—	4.86	4.89
8682.983	1.067	-1.568	10.700	—	4.86	4.89
8692.329	1.053	-1.653	5.200	—	4.86	4.89
8734.710	1.067	-2.018	4.100	—	4.87	4.90
Ti II						
4409.518	1.237	-2.530	38.100	—	4.90	4.89
4444.554	1.130	-2.103	59.900	—	4.90	4.90
4493.522	1.084	-2.604	31.800	—	4.86	4.86
4583.409	1.180	-2.664	30.200	—	4.96	4.96
4609.265	1.221	-3.797	11.600	—	4.91	4.91
4657.201	1.566	-2.466	51.800	—	4.93	4.92
4708.663	1.243	-2.174	50.600	—	4.95	4.95
4719.511	1.566	-3.496	12.200	—	4.99	4.99
4764.525	1.243	-2.514	33.500	—	4.93	4.93
4798.531	1.084	-2.484	42.900	—	4.94	4.94
4865.610	1.130	-2.603	35.000	—	4.85	4.85
5336.786	1.584	-1.299	72.000	—	4.91	4.90
5381.022	1.572	-1.572	56.600	—	4.94	4.93
5418.768	1.584	-1.829	48.100	—	4.94	4.94
HD84937						
Ti I						
2646.634	0.813	-0.417	16.723	0.881	3.22	3.46
2956.132	0.813	-0.357	15.147	0.708	3.05	3.30
3186.451	0.021	0.156	18.269	0.249	3.19	3.44
3191.992	0.048	0.269	23.646	0.293	3.22	3.47
3354.633	0.048	0.219	20.764	0.327	3.18	3.42
3370.434	0.021	-0.254	7.455	0.183	3.10	3.36
3371.452	0.813	-0.247	24.541	0.311	3.18	3.43
3385.941	0.813	-0.657	10.698	0.197	3.11	3.37
3635.462	0.021	0.246	20.818	0.243	3.06	3.31

**Table A.1.** Lines considered in the analysis, including saturated lines that were removed during final abundance calculation. Error for equivalent widths was not available for the lines of the Sun from [Scott et al. \(2015\)](#).

Wavelength Å	$E_{exc}$ eV	$\log(gf)$	$W_\lambda$ mÅ	Error	Abundances	
					LTE	NLTE
3729.807	0.021	-0.134	12.278	0.169	3.11	3.34
3741.059	0.048	-0.041	15.099	0.198	3.10	3.34
3904.783	1.046	-0.549	6.148	0.145	3.13	3.33
3924.526	0.048	-0.761	4.474	0.137	3.21	3.44
3947.768	0.048	-0.781	4.528	0.133	3.23	3.46
3958.205	0.813	-0.587	21.996	0.241	3.28	3.49
3989.758	0.048	-0.021	20.710	0.235	3.24	3.46
3998.636	0.813	-0.457	22.842	0.249	3.17	3.40
4008.927	0.048	-0.891	4.184	0.133	3.30	3.52
4024.571	0.813	-1.397	4.603	0.338	3.29	3.50
4287.403	0.848	-0.283	2.993	0.116	3.23	3.36
4305.907	0.900	0.147	20.131	0.231	3.32	3.44
4427.098	1.733	-0.247	2.837	0.180	3.20	3.38
4449.142	1.968	0.128	2.994	0.129	3.33	3.48
4518.022	0.836	-0.141	3.747	0.127	3.19	3.32
4533.239	0.900	0.198	17.596	0.200	3.18	3.31
4534.776	0.848	0.437	12.076	0.158	3.16	3.29
4535.569	0.836	0.249	9.021	0.143	3.21	3.34
4548.764	0.836	-0.171	4.395	0.144	3.29	3.41
4555.483	0.900	-0.742	2.536	0.115	3.18	3.31
4617.269	1.873	0.440	2.982	0.111	3.22	3.39
4981.731	0.900	0.228	20.401	0.190	3.21	3.34
4991.066	0.848	0.537	16.413	0.361	3.20	3.33
4999.503	0.836	0.429	13.348	0.168	3.21	3.34
5022.868	0.836	-0.221	2.989	0.115	3.14	3.28
5036.464	1.460	0.249	4.104	0.117	3.37	3.53
5173.743	0.021	-0.914	3.627	0.111	3.20	3.45
5192.969	0.048	-0.841	4.682	0.113	3.23	3.48
Ti II						
2474.194	0.113	-2.818	22.823	1.818	3.44	3.45
2517.431	0.151	-1.403	53.129	4.940	3.58	3.58
2571.032	1.080	-1.201	62.659	7.945	3.74	3.71
2581.711	1.116	-1.455	22.415	1.166	3.49	3.50
2717.297	1.161	-2.189	26.340	5.347	3.52	3.52
2725.773	1.130	-1.453	20.050	1.534	3.40	3.41
2761.287	1.084	-1.174	23.567	0.923	3.27	3.29
2784.638	1.080	-2.291	11.026	0.900	3.03	3.04
2820.361	0.607	-1.785	21.286	0.834	3.29	3.30
2832.176	0.607	-0.725	65.543	2.287	3.65	3.62
2841.935	1.080	-0.891	58.541	3.441	3.19	3.19
2862.319	1.243	-0.354	49.528	4.582	3.35	3.37
2884.102	1.161	-0.929	60.614	1.318	3.35	3.32
3017.183	1.892	-0.379	48.744	0.907	3.36	3.36
3029.728	1.582	-0.572	38.428	0.968	3.08	3.11
3046.684	1.180	-0.634	40.677	1.121	3.23	3.25
3056.738	1.165	-0.489	42.627	1.063	3.27	3.28
3058.088	1.221	-0.897	54.899	1.022	3.32	3.31
3071.239	1.221	-1.227	52.036	0.632	3.49	3.49
3089.400	2.048	-0.522	42.717	0.454	3.06	3.12
3103.803	1.893	0.083	51.629	0.712	3.24	3.30
3105.080	1.231	-0.129	52.530	0.787	3.27	3.27
3106.231	1.566	-0.246	56.670	0.543	3.07	3.08
3110.080	1.584	-0.909	12.605	1.576	3.16	3.19
3117.666	1.237	-0.490	41.388	1.879	2.98	3.01
3122.070	1.243	-1.394	11.697	0.540	3.16	3.18
3144.719	0.122	-2.184	24.452	1.897	3.35	3.35
3154.192	0.122	-0.984	69.833	0.771	3.56	3.49



**Table A.1.** Lines considered in the analysis, including saturated lines that were removed during final abundance calculation. Error for equivalent widths was not available for the lines of the Sun from [Scott et al. \(2015\)](#).

Wavelength Å	$E_{exc}$ eV	$\log(gf)$	$W_\lambda$ mÅ	Error	Abundances	
					LTE	NLTE
3184.117	0.028	-2.395	18.383	0.716	3.23	3.23
3197.519	0.049	-1.843	41.150	0.474	3.30	3.28
3203.431	0.012	-1.644	52.780	1.610	3.48	3.44
3213.121	0.028	-2.155	26.246	0.873	3.21	3.21
3214.767	0.113	-1.768	67.276	0.971	3.60	3.51
3224.237	1.892	-0.029	53.705	0.554	3.12	3.11
3226.769	0.049	-1.693	52.173	0.718	3.46	3.42
3236.119	1.084	-0.234	53.626	5.112	3.07	3.10
3249.366	1.084	-1.174	27.618	0.442	3.30	3.32
3263.683	1.180	-0.964	26.920	0.394	3.15	3.18
3272.077	1.231	0.051	51.744	1.237	3.02	3.06
3275.290	1.084	-1.304	16.020	0.224	3.08	3.11
3278.288	1.237	-0.260	58.420	0.502	3.26	3.28
3279.988	1.130	-1.093	28.995	0.699	3.21	3.23
3282.327	1.231	-0.039	52.539	0.561	3.14	3.17
3302.095	0.574	-2.562	20.723	0.304	3.24	3.23
3307.721	0.135	-2.535	12.661	0.204	3.25	3.24
3308.803	0.151	-1.143	68.140	0.518	3.54	3.49
3309.496	-5.761	0.032	11.933	0.190	3.14	3.18
3315.322	1.231	-0.339	44.200	0.578	3.17	3.20
3318.023	0.135	-0.945	73.533	0.530	3.55	3.49
3319.081	0.151	-2.903	7.573	0.178	3.33	3.33
3337.847	1.243	-1.074	19.774	0.279	3.11	3.15
3343.762	0.574	-1.402	69.415	0.495	3.54	3.48
3352.069	1.224	-1.280	22.323	0.298	3.20	3.23
3369.203	1.237	-1.420	15.098	0.212	3.12	3.15
3374.346	1.243	-0.884	28.908	3.204	3.18	3.20
3388.751	1.243	-0.844	27.381	0.364	3.10	3.13
3407.202	0.113	-2.368	39.785	0.969	3.28	3.27
3409.808	0.049	-1.813	43.641	0.506	3.30	3.29
3416.957	1.243	-1.364	11.353	0.230	3.09	3.12
3452.465	2.061	-0.259	15.914	0.262	3.03	3.10
3456.384	2.590	0.191	30.175	0.368	3.01	3.10
3461.496	0.151	-0.753	82.020	7.164	3.60	3.49
3477.180	0.135	-0.825	80.637	1.814	3.63	3.53
3489.736	0.151	-1.903	42.603	0.469	3.43	3.42
3491.049	0.122	-0.924	74.271	0.491	3.56	3.48
3500.333	0.135	-1.915	32.866	0.354	3.22	3.22
3504.891	1.893	0.283	56.694	1.011	3.12	3.10
3520.252	2.061	0.121	26.988	0.310	2.98	3.05
3533.854	2.590	-1.009	2.634	0.151	2.91	2.96
3535.407	2.590	0.311	32.222	0.321	2.94	3.02
3561.576	0.607	-1.915	17.707	0.465	3.21	3.21
3573.732	0.607	-1.405	35.625	1.841	3.20	3.19
3596.047	1.080	-1.371	53.092	0.638	3.26	3.21
3741.638	1.584	0.231	59.641	0.677	3.11	3.14
3757.685	1.572	-0.042	45.258	0.503	3.08	3.12
3759.291	1.080	-0.021	118.779	0.718	3.35	3.25
3761.321	0.607	0.305	112.735	0.673	3.32	3.22
3761.872	2.598	-0.545	9.989	0.157	2.97	3.01
3786.323	1.080	-2.901	8.811	0.556	3.31	3.31
3813.388	1.080	-2.191	27.090	0.289	3.22	3.22
3900.539	1.161	-0.989	80.301	0.528	3.49	3.38
3987.606	1.080	-3.031	5.331	0.142	3.18	3.18
4012.384	0.607	-1.655	38.560	0.369	3.32	3.31
4025.077	-4.668	-0.818	19.407	0.203	3.21	3.21
4028.338	1.893	-1.017	17.673	0.216	3.14	3.17

**Table A.1.** Lines considered in the analysis, including saturated lines that were removed during final abundance calculation. Error for equivalent widths was not available for the lines of the Sun from [Scott et al. \(2015\)](#).

Wavelength Å	$E_{exc}$ eV	$\log(gf)$	$W_\lambda$ mÅ	Error	Abundances	
					LTE	NLTE
4053.821	2.048	-1.672	13.115	0.171	3.12	3.15
4161.529	1.116	-1.965	8.613	0.148	3.19	3.19
4163.644	2.598	-0.255	23.253	0.242	3.13	3.17
4171.904	3.095	-0.476	18.053	0.208	3.15	3.20
4290.215	1.180	-0.694	53.161	0.593	3.27	3.24
4300.043	1.221	-0.937	72.296	0.782	3.39	3.31
4301.923	1.165	-0.909	38.264	0.418	3.25	3.25
4312.860	1.221	-1.597	42.831	0.503	3.28	3.27
4316.794	2.061	-1.319	3.773	0.122	3.19	3.23
4320.950	1.180	-1.704	13.552	0.406	3.27	3.27
4391.026	1.237	-2.300	6.717	0.141	3.39	3.39
4395.839	1.566	-2.106	9.203	0.146	3.18	3.19
4409.518	1.237	-2.530	2.082	0.116	3.09	3.10
4418.331	1.243	-1.814	8.415	0.142	3.20	3.20
4443.801	1.084	-0.534	69.175	0.448	3.43	3.34
4444.554	1.130	-2.103	6.948	0.131	3.20	3.20
4468.493	1.161	-1.329	71.117	0.462	3.45	3.34
4488.324	3.663	-0.500	4.765	0.133	3.14	3.19
4493.522	1.084	-2.604	1.934	0.111	3.16	3.16
4501.270	1.130	-0.673	65.839	0.474	3.42	3.34
4518.332	1.084	-2.384	4.121	0.132	3.28	3.28
4545.133	1.161	-3.149	3.986	0.133	3.20	3.20
4571.971	1.582	-0.532	63.803	0.423	3.33	3.25
4583.409	1.180	-2.664	1.789	0.103	3.26	3.26
4657.201	1.566	-2.466	4.909	0.147	3.23	3.23
4708.663	1.243	-2.174	4.197	0.114	3.21	3.21
4762.778	1.116	-2.765	1.443	0.119	3.13	3.13
4763.883	1.224	-2.400	4.295	0.120	3.25	3.26
4764.525	1.243	-2.514	2.066	0.106	3.23	3.23
4798.531	1.084	-2.484	2.612	0.198	3.16	3.16
4911.194	3.663	-0.640	3.448	0.110	3.11	3.20
5013.686	1.584	-1.839	4.012	0.136	3.28	3.28
5129.156	1.893	-1.437	9.976	0.154	3.19	3.18
5185.902	2.048	-2.012	8.391	0.136	3.17	3.17
5211.530	2.598	-1.535	1.205	0.097	2.92	2.99
5336.786	1.584	-1.299	10.452	0.138	3.18	3.17
5381.022	1.572	-1.572	5.299	0.141	3.20	3.20
5418.768	1.584	-1.829	3.676	0.153	3.21	3.20
HD140283						
Ti I						
2646.634	0.813	-0.417	21.293	0.479	2.81	3.06
3191.992	0.048	0.269	25.781	0.429	2.69	2.97
3199.914	0.813	-0.167	28.752	0.341	2.65	2.94
3354.633	0.048	0.219	22.144	0.310	2.62	2.90
3370.434	0.021	-0.254	9.251	0.198	2.62	2.89
3371.452	0.813	-0.247	25.988	0.317	2.62	2.90
3385.941	0.813	-0.657	11.835	0.210	2.57	2.85
3635.462	0.021	0.246	24.615	0.323	2.60	2.86
3729.807	0.021	-0.134	14.543	0.190	2.65	2.90
3741.059	0.048	-0.041	18.645	0.246	2.67	2.92
3904.783	1.046	-0.549	6.980	0.147	2.72	2.95
3924.526	0.048	-0.761	4.706	0.152	2.69	2.94
3947.768	0.048	-0.781	5.038	0.150	2.74	2.98
3958.205	0.813	-0.587	22.101	0.221	2.74	3.00
3981.762	0.021	-0.124	25.044	0.268	2.92	3.14
3989.758	0.048	-0.021	22.249	0.317	2.73	2.98

**Table A.1.** Lines considered in the analysis, including saturated lines that were removed during final abundance calculation. Error for equivalent widths was not available for the lines of the Sun from [Scott et al. \(2015\)](#).

Wavelength Å	$E_{exc}$ eV	$\log(gf)$	$W_\lambda$ mÅ	Error	Abundances	
					LTE	NLTE
3998.636	0.813	-0.457	25.204	0.273	2.68	2.94
4008.927	0.048	-0.891	4.274	0.133	2.76	3.01
4024.571	0.813	-1.397	3.899	0.172	2.67	2.92
4287.403	0.848	-0.283	1.681	0.107	2.50	2.65
4449.142	1.968	0.128	2.543	0.107	2.86	3.02
4518.022	0.836	-0.141	2.945	0.116	2.60	2.75
4533.239	0.900	0.198	16.912	0.177	2.68	2.82
4534.776	0.848	0.437	11.320	0.158	2.64	2.79
4535.569	0.836	0.249	7.941	0.142	2.67	2.81
4548.764	0.836	-0.171	3.542	0.119	2.71	2.85
4555.483	0.900	-0.742	2.533	0.108	2.70	2.85
4617.269	1.873	0.440	2.450	0.101	2.73	2.90
4981.731	0.900	0.228	18.916	0.195	2.69	2.83
4991.066	0.848	0.537	15.790	0.229	2.69	2.84
4999.503	0.836	0.429	12.664	0.166	2.69	2.84
5022.868	0.836	-0.221	3.346	0.096	2.71	2.86
5173.743	0.021	-0.914	3.636	0.102	2.65	2.93
5192.969	0.048	-0.841	5.308	0.105	2.73	3.00
Ti II						
2474.194	0.113	-2.818	16.588	0.479	2.77	2.78
2571.032	1.080	-1.201	49.930	1.408	2.82	2.82
2725.773	1.130	-1.453	16.545	0.478	2.88	2.89
2761.287	1.084	-1.174	17.913	0.362	2.69	2.71
2784.638	1.080	-2.291	11.018	0.339	2.59	2.60
2832.176	0.607	-0.725	73.872	0.669	3.40	3.38
2841.935	1.080	-0.891	57.579	0.633	2.63	2.66
2862.319	1.243	-0.354	39.353	0.691	2.60	2.65
2884.102	1.161	-0.929	53.627	0.743	2.62	2.64
2888.929	0.607	-1.235	35.823	1.749	2.67	2.70
3029.728	1.582	-0.572	35.125	0.496	2.59	2.63
3046.684	1.180	-0.634	33.755	0.442	2.61	2.65
3056.738	1.165	-0.489	39.140	0.490	2.72	2.75
3058.088	1.221	-0.897	46.472	0.431	2.58	2.62
3089.400	2.048	-0.522	36.812	0.592	2.51	2.57
3103.803	1.893	0.083	39.238	0.476	2.46	2.54
3105.080	1.231	-0.129	45.552	0.652	2.59	2.63
3106.231	1.566	-0.246	56.597	0.684	2.59	2.63
3110.080	1.584	-0.909	9.683	0.737	2.64	2.68
3154.192	0.122	-0.984	74.321	0.566	3.12	3.08
3184.117	0.028	-2.395	20.083	0.383	2.78	2.77
3195.715	1.116	-1.265	17.194	0.538	2.62	2.67
3197.519	0.049	-1.843	43.688	1.099	2.83	2.82
3203.431	0.012	-1.644	52.338	1.250	2.93	2.90
3213.121	0.028	-2.155	29.684	0.979	2.78	2.78
3224.237	1.892	-0.029	49.048	0.612	2.53	2.57
3226.769	0.049	-1.693	53.110	1.526	2.94	2.91
3263.683	1.180	-0.964	23.765	0.297	2.64	2.69
3272.077	1.231	0.051	52.508	1.251	2.56	2.62
3275.290	1.084	-1.304	16.374	0.279	2.67	2.71
3276.992	0.135	-2.315	16.969	0.235	2.69	2.69
3278.288	1.237	-0.260	50.905	0.561	2.53	2.59
3279.988	1.130	-1.093	22.024	0.275	2.59	2.63
3282.327	1.231	-0.039	47.776	0.533	2.52	2.57
3302.095	0.574	-2.562	19.755	0.248	2.71	2.71
3307.721	0.135	-2.535	14.970	0.215	2.84	2.84
3308.803	0.151	-1.143	66.696	0.739	2.91	2.89
3309.496	-5.761	0.032	12.151	0.208	2.72	2.77



**Table A.1.** Lines considered in the analysis, including saturated lines that were removed during final abundance calculation. Error for equivalent widths was not available for the lines of the Sun from [Scott et al. \(2015\)](#).

Wavelength Å	$E_{exc}$ eV	$\log(gf)$	$W_\lambda$ mÅ	Error	Abundances	
					LTE	NLTE
3315.322	1.231	-0.339	39.956	0.449	2.60	2.67
3318.023	0.135	-0.945	72.373	0.513	2.91	2.88
3319.081	0.151	-2.903	7.919	0.193	2.86	2.86
3337.847	1.243	-1.074	17.151	0.226	2.61	2.65
3343.762	0.574	-1.402	68.002	0.475	2.89	2.87
3352.069	1.224	-1.280	21.122	0.274	2.75	2.79
3369.203	1.237	-1.420	13.929	0.219	2.66	2.69
3374.346	1.243	-0.884	24.712	3.943	2.64	2.68
3407.202	0.113	-2.368	44.831	0.623	2.86	2.86
3409.808	0.049	-1.813	45.101	0.538	2.79	2.78
3416.957	1.243	-1.364	9.988	0.204	2.61	2.65
3452.465	2.061	-0.259	11.867	0.266	2.52	2.60
3456.384	2.590	0.191	24.325	0.288	2.49	2.59
3461.496	0.151	-0.753	80.096	5.435	2.90	2.85
3489.736	0.151	-1.903	46.395	0.573	3.00	3.00
3491.049	0.122	-0.924	71.993	0.686	2.86	2.82
3500.333	0.135	-1.915	35.313	0.400	2.75	2.75
3504.891	1.893	0.283	49.854	0.624	2.47	2.52
3520.252	2.061	0.121	21.796	0.483	2.47	2.55
3533.854	2.590	-1.009	3.172	0.148	2.64	2.69
3535.407	2.590	0.311	27.127	0.313	2.43	2.53
3561.576	0.607	-1.915	15.988	0.270	2.68	2.68
3573.732	0.607	-1.405	35.594	2.193	2.69	2.70
3596.047	1.080	-1.371	52.056	0.556	2.68	2.68
3741.638	1.584	0.231	53.184	0.610	2.56	2.63
3757.685	1.572	-0.042	37.523	0.387	2.54	2.61
3759.291	1.080	-0.021	111.636	0.687	2.75	2.66
3761.321	0.607	0.305	108.670	0.656	2.76	2.67
3761.872	2.598	-0.545	8.304	0.153	2.61	2.65
3786.323	1.080	-2.901	8.394	0.529	2.86	2.87
3813.388	1.080	-2.191	25.384	0.279	2.75	2.75
3900.539	1.161	-0.989	69.866	0.725	2.76	2.70
3913.461	1.130	-0.263	65.483	1.049	2.68	2.64
3981.991	0.607	-2.415	8.381	0.143	2.75	2.75
3987.606	1.080	-3.031	5.223	0.142	2.75	2.75
4012.384	0.607	-1.655	34.284	0.336	2.79	2.79
4025.077	-4.668	-0.818	18.395	0.199	2.75	2.75
4028.338	1.893	-1.017	12.998	0.195	2.65	2.70
4053.821	2.048	-1.672	9.145	0.147	2.62	2.67
4161.529	1.116	-1.965	7.348	0.147	2.73	2.74
4163.644	2.598	-0.255	14.121	0.184	2.58	2.65
4171.904	3.095	-0.476	10.990	0.155	2.63	2.69
4290.215	1.180	-0.694	46.801	0.436	2.71	2.72
4300.043	1.221	-0.937	67.900	0.754	2.84	2.81
4301.923	1.165	-0.909	38.424	0.525	2.87	2.87
4316.794	2.061	-1.319	2.012	0.104	2.61	2.67
4320.950	1.180	-1.704	11.160	0.171	2.79	2.80
4330.698	1.221	-2.567	6.467	0.124	2.75	2.76
4418.331	1.243	-1.814	7.433	0.138	2.76	2.78
4443.801	1.084	-0.534	61.977	0.401	2.82	2.76
4444.554	1.130	-2.103	5.172	0.115	2.68	2.68
4450.482	1.116	-1.395	24.059	0.262	2.76	2.75
4468.493	1.161	-1.329	64.215	0.414	2.84	2.78
4488.324	3.663	-0.500	1.828	0.100	2.49	2.53
4493.522	1.084	-2.604	1.295	0.096	2.60	2.61
4501.270	1.130	-0.673	58.311	0.390	2.81	2.77
4518.332	1.084	-2.384	3.297	0.114	2.79	2.80

**Table A.1.** Lines considered in the analysis, including saturated lines that were removed during final abundance calculation. Error for equivalent widths was not available for the lines of the Sun from [Scott et al. \(2015\)](#).

Wavelength Å	$E_{exc}$ eV	$\log(gf)$	$W_\lambda$ mÅ	Error	Abundances	
					LTE	NLTE
4545.133	1.161	-3.149	3.575	0.107	2.77	2.78
4571.971	1.582	-0.532	53.657	0.361	2.69	2.67
4583.409	1.180	-2.664	1.635	0.099	2.84	2.84
4657.201	1.566	-2.466	3.385	0.103	2.69	2.69
4708.663	1.243	-2.174	3.855	0.113	2.80	2.80
4763.883	1.224	-2.400	3.939	0.104	2.84	2.85
4764.525	1.243	-2.514	1.504	0.102	2.71	2.72
4798.531	1.084	-2.484	2.616	0.167	2.77	2.78
5013.686	1.584	-1.839	2.117	0.103	2.64	2.67
5129.156	1.893	-1.437	6.935	0.136	2.69	2.70
5185.902	2.048	-2.012	4.998	0.104	2.60	2.62
5211.530	2.598	-1.535	1.178	0.085	2.65	2.72
5336.786	1.584	-1.299	7.759	0.118	2.68	2.69
5381.022	1.572	-1.572	3.967	0.104	2.72	2.73
5418.768	1.584	-1.829	3.381	0.105	2.82	2.82
Arcturus						
Ti I						
4759.270	2.267	0.430	112.543	1.788	4.77	4.74
4778.255	2.239	-0.827	84.851	1.277	5.02	4.98
4913.613	1.879	0.329	137.628	2.769	5.14	5.09
4915.229	1.968	-1.253	72.443	0.911	4.80	4.74
4926.148	0.826	-1.944	93.792	0.497	4.87	4.83
4997.097	0.021	-1.924	167.350	8.078	5.45	5.48
4999.503	0.836	0.429	238.316	8.286	4.69	4.67
5009.645	0.048	-2.091	159.203	6.120	5.41	5.44
5016.161	0.900	-0.823	174.672	3.573	4.95	4.93
5024.844	0.826	-0.384	176.244	5.328	4.99	4.97
5043.584	0.848	-1.503	123.686	5.131	5.04	5.02
5145.460	1.502	-0.540	135.898	7.219	5.20	5.15
5147.478	0.021	-1.794	181.900	11.725	5.63	5.65
5230.967	2.249	-0.626	29.035	0.177	4.69	4.66
5282.376	1.067	-1.588	101.973	0.890	5.04	5.02
5300.010	1.067	-2.078	75.916	0.836	4.99	4.98
5338.306	0.836	-2.621	67.137	1.479	4.91	4.88
5366.639	0.826	-2.314	75.554	2.440	4.78	4.74
5384.630	0.836	-2.661	57.245	0.779	4.78	4.75
5453.642	1.460	-1.491	76.460	2.076	4.85	4.80
5465.773	1.430	-2.910	29.690	0.205	4.76	4.75
5471.192	1.460	-1.311	88.090	0.473	4.89	4.82
5866.451	1.430	-0.790	162.541	2.731	5.08	5.06
5918.536	1.430	-1.640	111.474	0.589	4.94	4.92
5922.110	1.053	-0.903	127.487	1.442	4.93	4.94
5937.809	1.430	-1.940	95.440	0.507	4.91	4.92
6091.171	2.289	-1.274	87.629	0.475	4.92	4.84
6336.099	1.460	-1.581	77.201	0.419	4.86	4.79
6395.472	1.733	-3.017	22.009	0.152	4.78	4.76
6497.684	1.460	-1.911	65.279	0.363	4.97	4.92
6554.223	1.460	-1.041	117.196	0.666	4.99	4.89
6556.062	1.502	-1.060	128.324	1.458	5.11	5.02
8692.329	1.053	-1.653	110.286	2.062	4.94	4.86
Ti II						
4798.531	1.084	-2.484	106.218	12.979	5.06	5.06
4865.610	1.130	-2.603	107.891	2.043	5.18	5.18
4874.009	3.123	-0.684	57.401	0.589	4.93	4.79
5005.167	1.572	-2.332	68.903	2.361	4.93	4.92
5211.530	2.598	-1.535	65.531	1.450	4.93	4.92

**Table A.1.** Lines considered in the analysis, including saturated lines that were removed during final abundance calculation. Error for equivalent widths was not available for the lines of the Sun from [Scott et al. \(2015\)](#).

Wavelength Å	$E_{exc}$ eV	$\log(gf)$	$W_\lambda$ mÅ	Error	Abundances	
					LTE	NLTE
HD122563						
Ti I						
3598.714	1.046	-1.309	9.777	0.220	2.35	2.74
3725.152	1.430	-0.340	4.023	0.142	1.84	2.19
3729.807	0.021	-0.134	62.128	0.445	2.06	2.42
3741.059	0.048	-0.041	60.851	0.428	1.91	2.30
3752.858	0.813	-0.427	74.038	0.929	2.03	2.40
3904.783	1.046	-0.549	26.459	0.363	2.05	2.51
3924.526	0.048	-0.761	29.245	0.373	2.03	2.40
3947.768	0.048	-0.781	31.212	0.770	2.09	2.44
3958.205	0.813	-0.587	73.019	2.408	2.10	2.48
3998.636	0.813	-0.457	75.584	1.503	2.01	2.40
4008.927	0.048	-0.891	26.877	0.330	2.10	2.44
4287.403	0.848	-0.283	19.025	0.231	2.25	2.48
4449.142	1.968	0.128	5.708	0.152	2.10	2.35
4518.022	0.836	-0.141	18.905	0.202	2.09	2.33
4534.776	0.848	0.437	43.721	0.333	2.00	2.25
4535.569	0.836	0.249	36.210	0.479	2.07	2.31
4548.764	0.836	-0.171	17.749	0.190	2.08	2.32
4555.483	0.900	-0.742	13.090	0.158	2.08	2.32
4617.269	1.873	0.440	8.111	0.138	2.11	2.37
4981.731	0.900	0.228	62.468	0.396	2.04	2.30
5022.868	0.836	-0.221	17.917	0.195	2.09	2.34
5036.464	1.460	0.249	12.377	0.162	2.20	2.51
5173.743	0.021	-0.914	32.679	0.316	2.10	2.46
5192.969	0.048	-0.841	37.243	0.333	2.09	2.46
Ti II						
3500.333	0.135	-1.915	99.922	2.727	2.68	2.70
3533.854	2.590	-1.009	15.915	0.250	2.30	2.34
3535.407	2.590	0.311	66.974	1.476	2.10	2.19
3757.685	1.572	-0.042	83.136	2.103	2.20	2.33
3759.291	1.080	-0.021	209.168	1.279	2.62	2.62
3761.321	0.607	0.305	194.250	4.133	2.56	2.57
3761.872	2.598	-0.545	34.370	0.552	2.38	2.44
3774.647	0.607	-2.525	55.363	3.764	2.61	2.63
3776.053	1.584	-0.939	51.734	0.689	2.36	2.43
3813.388	1.080	-2.191	100.697	5.068	2.88	2.91
3900.539	1.161	-0.989	133.115	0.853	2.74	2.72
3987.606	1.080	-3.031	48.878	0.636	2.58	2.58
4012.384	0.607	-1.655	103.308	2.660	2.73	2.74
4025.077	-4.668	-0.818	90.895	0.846	2.77	2.78
4028.338	1.893	-1.017	54.402	0.386	2.42	2.48
4053.821	2.048	-1.672	41.757	0.460	2.34	2.40
4161.529	1.116	-1.965	51.710	0.594	2.54	2.56
4163.644	2.598	-0.255	45.062	0.480	2.28	2.35
4316.794	2.061	-1.319	18.131	0.207	2.54	2.60
4330.698	1.221	-2.567	49.565	0.624	2.60	2.61
4391.026	1.237	-2.300	46.454	0.470	2.80	2.80
4395.839	1.566	-2.106	51.120	0.621	2.53	2.55
4409.518	1.237	-2.530	21.144	0.293	2.54	2.56
4418.331	1.243	-1.814	51.096	0.348	2.58	2.60
4444.554	1.130	-2.103	47.123	0.503	2.57	2.58
4488.324	3.663	-0.500	10.120	0.159	2.38	2.41
4493.522	1.084	-2.604	18.654	0.202	2.53	2.55
4518.332	1.084	-2.384	32.997	0.353	2.63	2.65
4545.133	1.161	-3.149	33.627	0.282	2.59	2.61



**Table A.1.** Lines considered in the analysis, including saturated lines that were removed during final abundance calculation. Error for equivalent widths was not available for the lines of the Sun from [Scott et al. \(2015\)](#).

Wavelength Å	$E_{exc}$ eV	$\log(gf)$	$W_\lambda$ mÅ	Error	Abundances	
					LTE	NLTE
4583.409	1.180	-2.664	16.976	0.221	2.64	2.65
4609.265	1.221	-3.797	5.332	0.116	2.58	2.59
4657.201	1.566	-2.466	34.988	0.629	2.59	2.60
4708.663	1.243	-2.174	36.021	0.280	2.65	2.66
4719.511	1.566	-3.496	6.008	0.130	2.70	2.71
4763.883	1.224	-2.400	35.184	0.346	2.66	2.68
4764.525	1.243	-2.514	18.544	0.198	2.60	2.62
4798.531	1.084	-2.484	28.559	0.650	2.62	2.63
4865.610	1.130	-2.603	24.999	0.249	2.62	2.63
4874.009	3.123	-0.684	4.867	0.123	2.35	2.40
4911.194	3.663	-0.640	8.161	0.129	2.40	2.45
5013.686	1.584	-1.839	22.092	0.212	2.55	2.57
5129.156	1.893	-1.437	40.354	0.823	2.48	2.50
5185.902	2.048	-2.012	35.635	0.319	2.47	2.49
5211.530	2.598	-1.535	5.966	0.111	2.38	2.46
5336.786	1.584	-1.299	53.625	0.370	2.56	2.58
5381.022	1.572	-1.572	34.910	0.280	2.60	2.61
5396.247	1.892	-3.259	5.427	0.112	2.88	2.89
5418.768	1.584	-1.829	26.487	0.208	2.61	2.62